Journal of Engineering Science and Technology
Vol. 13, No. 10 (2018) 3393 - 3418

ENHANCED PARTICLE SWARM OPTIMIZATION BASED DC-LINK VOLTAGE CONTROL ALGORITHM FOR INTERLEAVED SAPF

VIJAYAKUMAR GALI*, NITIN GUPTA, R. A. GUPTA

Malaviya National Institute of Technology Jaipur,
JLN Marg, Malaviya Nagar, Jaipur, 302017, India
*Corresponding Author: vijaykumar209@gmail.com

Abstract

This paper investigates the intrinsic influence of DC-link capacitor voltage on the compensation performance of interleaved SAPF. PI controller has played a significant role in regulating the DC-link voltage to minimise the undesirable switching and interfacing inductor power losses. Its gain values will change continuously with the undesirable condition of load and supply voltages. PSO has used for tuning the PI controller gain values. However, this technique causes to local optimum with premature convergence, which resulted in poor performance in terms of overshoot, undershoot, settling time and accuracy. To address these issues, the idea of simulated annealing algorithm is used in proposed EPSO. This proposed algorithm reduces the convergence time by eliminating the premature particle's best position and comprehends the computational complexity. The proposed system is simulated by using MATLAB®/ Simulink software to validate the feasibility and effectiveness of proposed control algorithm in comparison with conventional PI and PSO based control algorithms under the steady state and transient condition of the load. The simulation results are validated by implementing a prototype in the laboratory. The proposed control technique achieved better performance in terms of dynamic response, 99.97% accuracy of DC-link voltage regulation, overshoot of 5V, and undershoot of 3 V, settling time of 0.05 seconds and accuracy in comparison with conventional algorithms.

Keywords: DC-link voltage regulation, Enhanced particle swarm optimisation (EPSO), Interleaved inverter based SAPF, Particle swarm optimization (PSO), Power quality, Shoot-through problems.

1. Introduction

The harmonic and reactive power compensations have become an essential requirement in the present power system scenario due to continuing the proliferation of power electronic devices. The modern power system has inevitable non-linear loads, which inject variable harmonics contents into the system. This harmonic pollution creates huge problems or malfunction of various equipment like humming noise in transformers, damage winding and insulation in electrical machines, create interferences in a telecommunication system, a false reading of digital meters, etc. [1-3].

Various solutions for mitigating different PQ problems such as passive filters, active filters and hybrid filters have presented in the literature. Active Power Filters (APFs) have attracted more as a proficient device to compensate power quality problems. Three types of active filters is available in the literature such as shunt, series-APF and Unified Power Quality Conditioner (UPQC). Shunt Active Power Filter (SAPF) is the most effective tool to mitigate current harmonics and reactive power. The Shunt APF is a Voltage Source Inverter (VSI) with a self-supported DC-link capacitor and connected parallel to the grid at the Point of Common Coupling (PCC) through filtering inductors [4, 5]. This conventional VSI encounters with one of the hazardous problems, i.e., shoot-through problem. According to Sun et al. [6], when the two switches of the same leg are switched on simultaneously, extreme current will flow through switches, which may damage the power switches. Chen and Peng [7] introduced dead time elimination PWM technique to solve the shoot-through problem by decomposing phase leg switches into two switching cells. It will be configured with the controllable switches and in series with the diode. However, the control scheme is complicated, which requires high-speed DSPs/ Microcontrollers, hence, increase the cost of the system. Goluszek [8] invented interleaved buck inverter to replace the conventional VSI topology with the advantage of eliminating the shoot-through problems by changing circuit configuration. Patel and Panda [9] and Panda and Patel [10] used interleaved buck inverter topology to overcome the problem of shoot-through in APFs and tested using OPAL-RT software. This topology is working successfully as SAPF without considering the effect of the shoot-through problem. However, the practical gird voltage conditions, load fluctuations and time-varying harmonics do not resemble in the OPAL-RT environment.

The proposed system can be implemented for the grid integration of renewable energy system. Where the system undergoes the unpredictable operation of load and supply. Any model in the Simulink model can be processed through three tests, i.e., Model In-The-Loop (MIL), Software-In-The-Loop (SIL) and Processor-in-the-Loop (PIL). MIL is a test conducted to verify the model in the MATLAB environment without any physical system presence. Once the model is passed the test in MIL, it goes to the SIL test. The SIL test is to be conducted to verify the algorithm within the embedded software in the host computer. After the SIL test, the PIL test can be conducted to test the model in the embedded target. Once all three tests completed, the controller is ready for the hardware testing [11].

In this paper, authors are implemented interleaved inverter based SAPF by using a dSPACE1104 controller over conventional VSI based SAPF.

Reference current generation techniques for interleaved SAPF play a crucial role in the harmonic compensation. However, the accuracy of reference current

impacts the compensation of different harmonics levels presented in the system [12-15]. The control techniques like Power Balance Theory (PBT) [16], Instantaneous Symmetrical Component Theory (ISCT) [17], Enhanced Phase Locked Loop (E-PLL) based control algorithm [18], Synchronous Reference (*d-q*) theory [19], Instantaneous Reactive Power Theory (IRPT) [20, 21], etc. Among these control techniques, IRPT also called *p-q* theory is attracted researchers because of its ease of implementation, effective compensation under sinusoidal supply voltage condition. The generalised *p-q* theory has been used in this paper for reference current generation.

The DC-link capacitor voltage plays a significant role in the compensation performance of active filters. It supplies the harmonic component of currents, switching losses, reactive power under steady state and real power under the transient condition of the load. During a transient condition of the load, there is a large variation in between reference and actual value of DC-link voltage. The DC-link voltage has to maintain at reference value under different load and supply voltage conditions [22, 23]. The Proportional-Integral (PI) controllers have been used in the industry because of its simple structure, low cost, less design complexity. The proportional gain value (k_p) helps to improve the system performance by reducing steady-state error and forced oscillations whereas integral gain value (k_i) enhance the overall system stability. The variable non-linear loads inject different harmonic components into the system, which violate the DC-link voltage from its reference value. Hence, this serious undesirable oscillations (overshoot and undershoot) lead to the dielectric breakdown of the DC-link capacitor under the transient condition of the load. In other hand, the DC-link capacitor has to supply instant, real power to meet the load requirement, which leads to a sharp decrement in DC-link capacitor voltage when load increased and vice versa [24, 25]. It is important for the controller to adopt the changes in the system to maintain the reference value. Therefore, tuning of PI controller gain values has become very much important for efficient operation of the interleaved shunt APF.

There are many methods available in the literature to tune the gain values of PI controllers. In 1942, Ziegler and Nichols were employed in the Tylor Instruments, developed a mathematical model for tuning of PI controller gain values. This method of tuning is having rugged response under the transient condition of load and supply voltages. Kumar and Mahajan [26] proposed various optimization techniques to optimise the PI controller gain values. The Fuzzy Logic Controller (FLC) have found to be an impressive tool because of its high robustness, insensitive to parameters changes, treating non-linearity, etc. However, this has disadvantages like (i) lack of process to select optimum no. of rules since various factors are involving in the assessment like performance of controller, compensation efficiency, choice of linguistic variables, etc., (ii) the knowledge of human operator is repeatedly inadequate and non-methodical, (iii) the rules are not assured to be coherent hence, arises mismatch between rules, and (iv) large computational time for fuzzification and defuzzification [27, 28]. The E. coli and M. Xanthus motivate bacterial foraging optimization (BFO) algorithm, foraging behaviour of bacteria that observes the chemical gradients in the environment and move towards or away from the specific signal. The enactment of the bacteria progressed into four sections, chemotaxis, swarming, reproduction, and elimination and dispersal [29-31]. The speed of the convergence to obtain maximum at the lower search space for saving the time and

memory is the big challenge for the researchers. Particle swarm optimization technique has been introduced by Eberhart and Kennedy in the year 1995 by understanding the swarming behaviour of the bird and fish flock. The PSO has advantages like solving multi-objective function, non-linearity and non-differentiability with the multi-diametrical problem. A swarm processed in the search space to discover optimal solutions. The particles in the search space try to reach its optimal solution by updating position on own best position obtained by each particle. Due to its simplicity, ease of implementation with low-cost controllers and a well-balanced mechanism to reach out local and global best, it became more popular in various applications [32-34]. However, it has disadvantages like exploring all local best position obtained by the all particles in the search space, which increase the complexity of the computation, reduce the speed of the processors and increase the no. of iterations. Based on a study by Tian and Shi [35], by considering the above issues of optimization problems, authors in this paper proposed Enhanced Particle Swarm Optimization (EPSO) technique to solve multi-objective function by eliminating the local best opposition and improve the converge speed obtained by the particles in the search space. In addition, the performance improvement is compared with conventional techniques.

This paper divided into five sections. Section 2 depicts interleaved inverter based SAPF system architecture and mathematical modelling for DC-link capacitor voltage stabilisation. Section 3 describes the impact of DC-link voltage stabilisation on compensation performance by enhanced PSO in comparison to the PI and conventional PSO techniques. The performance of the proposed control technique is tested in comparison with the conventional PI and PSO based controllers under steady state and transient condition of the load using the MATLAB®/ Simulink environment in Section 4. The simulation results are validated by developing the prototype model using the dPSCE1104 controller in the laboratory in Section 5 and followed by conclusions.

2. Interleaved Inverter based SAPF System Architecture

Figure 1 shows the hardware implementation block diagram of the proposed system. The interfacing inductors (L_{fa1}, L_{fa2}, L_{fb1}, L_{fb2}, $L_{fc1,}$ L_{fc2},) are used for removing the ripples in the compensating currents and act as a medium between the grid and active filter for transferring the energy. The smoothening inductor ($L_{se,a}$, $L_{se,b}$ $L_{se,c}$) are connected along with the diode bridge rectifier for eliminating higher frequency switching noise. The proposed inverter consists of six legs and each leg connected with a Metal-Oxide-Semiconductor Field Effective Transistor (MOSFET) and a fast recovery power diode. This type of construction avoids the shoot-through problem, which is a common phenomenon in the conventional VSI topology. The DC-link capacitor voltage (C_{dc}) is connected at the DC-side of the three-phase interleaved inverter to supply load reactive power and real power during the transient condition of the load.

3. Analysis of Minimum DC-Link Voltage Deduction

3.1. DC-link voltage stabilisation for three-phase three-wire interleaved inverter based SAPF

The DC-link voltage plays a remarkable role in the harmonic compensation process. In a practical scenario, the system harmonic currents vary frequently with a change

in non-linear loads. In steady-state operation, the real power supplied by the source is equal to load demand and power losses in the interleaved SAPF switches, inductors. There is a real power difference between the source and load demand during a transient condition of the load. The DC-link capacitor can supply this extra real power during a transient condition of the load. Hence, the DC-link capacitor acts as an energy source to maintain the energy balance in the interleaved SAPF.

The DC-link capacitor voltage has to be maintained its reference value irrespective of load changes. The objective function of minimum DC-link voltage requirement for three-phase interleaved inverter based SAPF can be derived from the circuit operation. The equivalent model of the proposed system is shown in Fig. 2. The following equation can be derived by applying Kirchhoff's voltage law as follows:

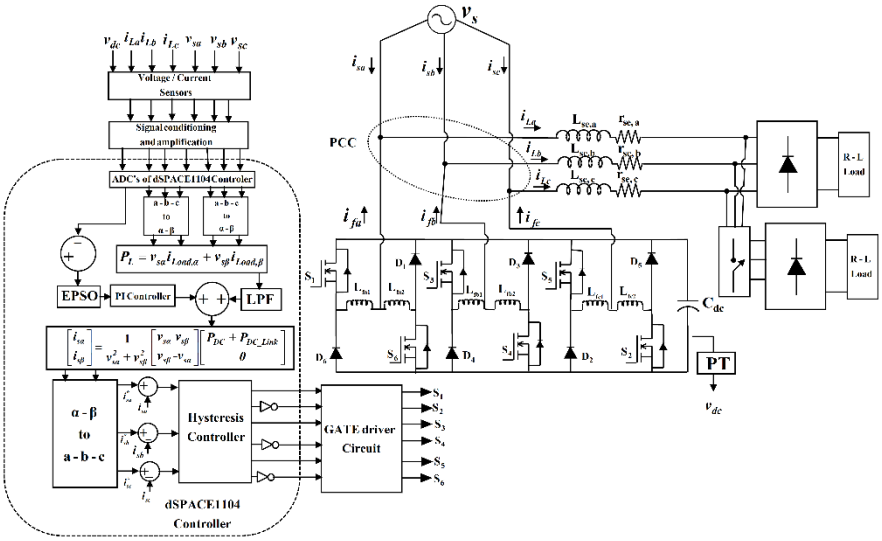

Fig. 1. Three-phase interleaved inverter based SAPF.

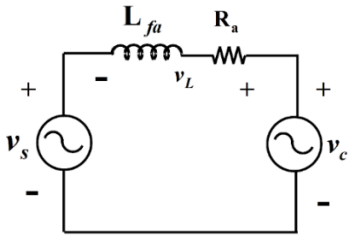

Fig. 2. Single-phase equivalent circuit model of the interleaved inverter based SAPF.

$$v_c = v_s + v_L \tag{1}$$

$$v_c = v_s + \mathrm{R_a} * i_{fa} + \mathrm{L_a} \frac{di_{fa}}{dt} \tag{2}$$

To simplify, the detailed analysis of the supply and inverter voltages are defined as follows:

$$v_s = \sqrt{2}\, V_{sn} \cos(\omega t + \phi_1) \tag{3}$$

$$v_c = V_{c1} \cos(\omega t + \varphi_1) + \sum_{n=2}^{\infty} V_{cn} \cos(n\omega t + \varphi_n) \tag{4}$$

where, V_{sn} is the peak value of supply voltage, V_{c1} and V_{cn} are the effective fundamental and n^{th} components of the inverter voltages, respectively. ω is the fundamental angular frequency, ϕ and φ signify the initial phase components of supply and inverter voltages, respectively. Assume that the non-linear load current (i_{Load}) consists of fundamental and harmonic components.

$$i_{Load} = i_{Load1} + i_{Load,h} \tag{5}$$

$$= I_{Load1} \cos(\omega t + \phi_1) + \sum_{n=2}^{\infty} I_{Load,n} \cos(n\omega t + \phi_{n1}) \tag{6}$$

where, I_{Load1} and $I_{Load,n}$ are the fundamental and n^{th} harmonic component of load current, respectively. Assume that the interleaved inverter based SAPF compensating current is composed of a fundamental i_{f1} and harmonic component i_{fh} of currents, respectively.

$$i_f = i_{f1} + i_{fh} \tag{7}$$

$$= i_{f1} \cos(\omega t + \phi_1) + \sum_{n=2}^{\infty} I_{f,n} \cos(n\omega t + \phi_n) \tag{8}$$

The fundamental component of interleaved inverter output current is very small ($i_{f1} \approx 0$) to maintain the DC-link voltage and system power loss under the steady state operation of the SAPF. Therefore, the fundamental interleaved inverter current can be neglected under steady-state operation. If the interleaved SAPF generates compensated currents whose magnitudes are equal to load harmonic currents, the total harmonics injected into the source vanishes. Therefore, the phase-*a* compensating current can be written as follows:

$$i_{fa} = i_{fa,h} = i_{Load,h} = \sum_{n=2}^{\infty} I_{\mathrm{Load},n} \cos(n\omega t + \phi_n) \tag{9}$$

The voltage equation can be written by substituting Eqs. (3), (4) and (9) in the Eq. (1).

$$\begin{aligned} &V_{c1}\cos(\omega t+\varphi_1)+\sum_{n=2}^{\infty}V_{cn}\cos(n\omega t+\varphi_n) \\ &=\sqrt{2}\,V_{sn}\cos(\omega t+\phi_1)+R_a*\sum_{n=2}^{\infty}I_{Load,n}\cos(n\omega t+\phi_n) \\ &\quad+L_a*\frac{\sum_{n=2}^{\infty}d\left\{I_{Load,n}\cos(n\omega t+\phi_n)\right\}}{dt} \end{aligned} \tag{10}$$

The supply voltage, interleaved inverter based SAPF output voltage and compensating current can be expressed according to Euler's formula as follows:

$$\left.\begin{aligned} \sqrt{2}\,V_{sn}\cos(\omega t+\phi_1) &= \sqrt{2}\,V_{sn}\,\mathrm{Re}\left\{e^{j(\omega t+\phi_1)}\right\} \\ V_{c1}\cos(\omega t+\varphi_1) &= V_{c1}\,\mathrm{Re}\left\{e^{j(\omega t+\varphi_1)}\right\} \\ \sum_{n=2}^{\infty}V_{cn}\cos(n\omega t+\varphi_n) &= \sum_{n=2}^{\infty}V_{cn}\,\mathrm{Re}\left\{e^{j(n\omega t+\varphi_1)}\right\} \\ \sum_{n=2}^{\infty}I_{Load,n}\cos(n\omega t+\phi_n) &= \sum_{n=2}^{\infty}I_{Load,n}\,\mathrm{Re}\left\{e^{j(n\omega t+\phi_1)}\right\} \end{aligned}\right\} \tag{11}$$

Substituting the Eq. (11) into the Eq. (10), the voltage equations will become as follows:

$$\left.\begin{aligned} &V_{c1}\,\mathrm{Re}\left\{e^{j(\omega t+\varphi_1)}\right\}+\sum_{n=2}^{\infty}V_{cn}\,\mathrm{Re}\left\{e^{j(n\omega t+\varphi_1)}\right\} \\ &=\sqrt{2}\,V_{sn}\,\mathrm{Re}\left\{e^{j(\omega t+\phi_1)}\right\}+R*\sum_{n=2}^{\infty}I_{Load,n}\,\mathrm{Re}\left\{e^{j(n\omega t+\phi_1)}\right\} \\ &\quad+L*\sum_{n=2}^{\infty}I_{Load,n}\,\mathrm{Re}\left\{jn\,\omega e^{j(n\omega t+\phi_1)}\right\} \end{aligned}\right\} \tag{12}$$

It is clear that the corresponding real parts on both sides of the equation are the same sinusoidal frequency vector. Hence, real parts symbol on both sides can be removed.

$$\left.\begin{aligned} &V_{c1}\left\{e^{j(\omega t+\varphi_1)}\right\}+\sum_{n=2}^{\infty}V_{cn}\left\{e^{j(n\omega t+\varphi_1)}\right\} \\ &=\sqrt{2}\,V_{sn}\left\{e^{j(\omega t+\phi_1)}\right\}+R*\sum_{n=2}^{\infty}I_{Load,n}\left\{e^{j(n\omega t+\phi_1)}\right\}+L*\sum_{n=2}^{\infty}I_{Load,n}\left\{jn\,\omega e^{j(n\omega t+\phi_1)}\right\} \end{aligned}\right\} \tag{13}$$

The real parts and imaginary parts on both sides are equal in Eq. (13). Thus, the following equation can be obtained:

$$\left.\begin{aligned} V_{c1} &= \sqrt{2}\, V_{sn} \\ \sum_{n=2}^{\infty} V_{cn} &= R^{*}\sum_{n=2}^{\infty} I_{Load,n} + \omega L^{*}\sum_{n=2}^{\infty} nI_{Load,n} \end{aligned}\right\} \tag{14}$$

The mould length of the interleaved inverter output voltage vector can be defined as follows:

$$V_c = \left\| V_{c1}\left\{e^{j(\omega t+\varphi_1)}\right\} + \sum_{n=2}^{\infty} V_{cn}\left\{e^{j(n\omega t+\varphi_1)}\right\} \right\| \tag{15}$$

The maximum mould length of the interleaved inverter output voltage can be expressed from Eqs. (14) and (15) in vector form as follows:

$$\left.\begin{aligned} V_{c\_max} &= V_{c1} + \sum_{n=2}^{\infty} V_{cn} \\ &= \sqrt{2}\, V_{sn} + R^{*}\sum_{n=2}^{\infty} I_{Load,n} + \omega L^{*}\sum_{n=2}^{\infty} nI_{Load,n} \end{aligned}\right\} \tag{16}$$

The efficient compensation is achieved by the interleaved inverter based SAPF if the sufficient DC-link voltage is to be supplied. The relation between interleaved inverter based SAPF output voltage and mould length can be defined as follows:

$$\left.\begin{aligned} V_{c\_min} &= \frac{2}{m} V_{c\_max} \\ &= \frac{2}{m}\left\{\sqrt{2}\, V_{sn} + R^{*}\sum_{n=2}^{\infty} I_{Load,n} + \omega L^{*}\sum_{n=2}^{\infty} n^{*} I_{Load,n}\right\} \end{aligned}\right\} \tag{17}$$

where m is the modulation index of the interleaved inverter. The interleaved inverter based SAPF produces maximum output voltage that higher than the maximal value of interleaved inverter voltage mould vector. Therefore, harmonics produced by the non-linear loads are compensated completely. The minimum DC-link voltage is derived by substituting Eq. (16) into Eq. (17) as follows:

$$\left.\begin{aligned} V_{dc\_min} &= \frac{2}{m} V_{c\_max} \\ &= \frac{2}{m}\left\{\sqrt{2}\, V_{sn} + R_a^{*}\sum_{n=2}^{\infty} I_{Load,n} + \omega L_a^{*}\sum_{n=2}^{\infty} n^{*} I_{Load,n}\right\} \end{aligned}\right\} \tag{18}$$

The important factors can be concluded from the Eq. (18) that the minimum DC-link voltage influenced by the supply voltages, interfacing inductors, effective resistance of inductor values, non-linear load currents and modulation index values.

Therefore, the stabilising the DC-link voltage is the key factor in the compensation process. The three-phase harmonic currents are independently compensated with three-phase three-wire interleaved inverter based SAPF. The equivalent DC-link voltage objective function can be written by considering the required minimum DC-link voltage for each of three-phases as follows:

$$V_{dc} = \max\left\{V_{dc,a\_min}, V_{dc,b\_min}, V_{dc,c\_min}\right\} \tag{19}$$

3.1.1. PI controller

As stated by Kazem [4], the compensation efficiency highly depends on the DC-link voltage stabilisation. The DC-link capacitor experiences the overshoot and undershoots under steady state and transient condition of the load. The PI controller minimises the switching losses, inductor losses, etc., and supply real power required by the load during the transient condition. The PI controller gain values have calculated by the conventional linearised model of the interleaved inverter based SAPF. The average energy stored in the DC-link capacitor can be calculated as:

$$W_{dc} = C_{dc}\frac{(V^{*}_{dc,avg})^2}{2} \tag{20}$$

where, $V^{*}_{dc,avg}$ is the average value of DC-link voltage and C_{dc} is the average value of capacitor values. The DC-link capacitor energy loss is calculated as:

$$\Delta W_{dc} = W^{*}_{dc} - W_{dc} = C_{dc}\frac{(V^{*}_{dc})^2 - (V^{*}_{dc,avg})^2}{2} \tag{21}$$

where, ΔW_{dc} is the energy loss, V^{*}_{dc} is the DC-link capacitor voltage.

The PI controller works efficiently to retain its reference value. The output of the PI controller can be acquired as follows:

$$\left.\begin{aligned} y(t) &= K_p.e(t) + K_i\int_0^t e(t).dt \\ &= K_p.[z(t) - c(t)] + K_i\int_0^t [z(t) - c(t)].dt \end{aligned}\right\} \tag{22}$$

Here, *z (t), c (t)* and *e (t)* are the PI controller desired output, actual output and generated error, respectively. The desired PI controller gain values are calculated by using Eq. (22). This equation gives the PI controller gain values in for particular load. However, the electrical distribution system experiences inevitable load changes. The gain parameters of the PI controller have to be tuned for different states of loads. Hence, tuning of PI controller gain values is a multi-objective function, which has to be tuned precisely. There are various optimisation techniques are available in the literature to overcome the problems of PI controller tuning. The conventional PSO and proposed EPSO based control techniques have been implemented and performance analysed in comparison with the conventional PI controller in this paper.

3.1.2. Conventional PSO based PI controller

The swarm intelligent techniques play an immense role to solve the multi-objective function of the non-linear system. Kennedy and Eberhart developed the Particle Swarm Optimisation (PSO) in 1995 [8]. It was inspired by observing the social behaviour of the bird flock or fish schooling. PSO employs based on the population of particles in the search space. The swarm is having N number of particles that search n-dimensionally in the search space to discover optimised solutions. Every particle in the search space explores its own best position and best swarm overall experience. The interleaved inverter based SAPF undergoes undesirable operation under the transient condition of the load, which increase the non-linearity in the system. The PSO has been recognised to be very proficient in solving non-linearity, non-differentiability, multiple objective function and multi-dimensional problems. It is comprehensively used because of its simple structure, ease of implementation, less computational burden and a well-defined mechanism to explore both local and global maxima. The following equations are used for updating the positions and velocities of the particles in accordance with the social only and cognition only components.

$$u_{k+1}^{i} = \chi u_{k}^{i} + \lambda_1 . c_1 (q_{Lbest}^{i} - x_{k}^{i}) + \lambda_2 . c_2 (q_{gbest}^{\ i} - x_{k}^{i}) \tag{23}$$

$$x_{k+1}^{i} = x_{k}^{i} (1 - \lambda_2) + \lambda_2 q_{gbest} + \eta\beta \tag{24}$$

where, q_{Lbest}^{i} and q_{Gbest}^{i} are local best and global best obtained by the particles, respectively. k and *i* are the no. of iterations and particle number, respectively. x_{k}^{i} and u_{k}^{i} are the present position and velocity of the i^{th} particle at k^{th} iteration, respectively. x_{k+1}^{i} and u_{k+1}^{i} are the position and velocity of the i^{th} particle at $(k+i)^{th}$ iteration. χ , λ_1 and λ_2 are the coefficient of inertia, cognitive and social constraints, respectively. The random numbers c_1 and c_2 are in the interval [-1, 1].

The speed of the particles are decided by the λ_1 and λ_2 , balance provided between local and global in the search space by χ . The search process will be terminated if the predefined maximum no. of iterations completed or additional best solution is not obtained. A complete flow chart of PSO is shown in Fig. 3. The number of iterations and increase no. of premature convergence of particle's best position will increase the complexity of the program and degrade the convergence speed. An Enhanced Particle Swarm Optimisation (EPSO) is proposed in this paper to overcome the problems of conventional PSO.

3.1.3. Proposed enhanced particle swarm optimization

In conventional PSO, the particle has the capability to know the best position obtained by all the group particles. The particle has to find the global best instead of finding local best positions obtained by the all group particles. By making some modifications in the conventional PSO by using a simulated annealing algorithm, the author in this paper has proposed Enhanced Particle Swarm Optimization (EPSO) algorithm. The EPSO eliminates premature convergence and reduces the computational complexity. This divided into two parts, firstly, it chooses maximum fitness particles while iterating and initializing the position arbitrarily. Therefore, the particle can choose more search domains. Secondly, the idea of simulating

annealing has been used to achieve the convergence PSO. It improves the convergence speed of the particle to obtain the best solution. The EPSO equations for the i^{th} particle's position after $(k+1)^{th}$ iterations can be written as follows:

$$x_{k+1}^{i} = x_{k}^{i}(1-\lambda_2) + \lambda_2 q_{gbest} + \eta\beta \tag{25}$$

where, η is the random number, which decreases after successive iterations and can be defined as follows:

$$\eta = \eta_0 e^{-\alpha t} \ (0< \alpha \ 1), \ (0.5< \alpha_0 <1) \tag{26}$$

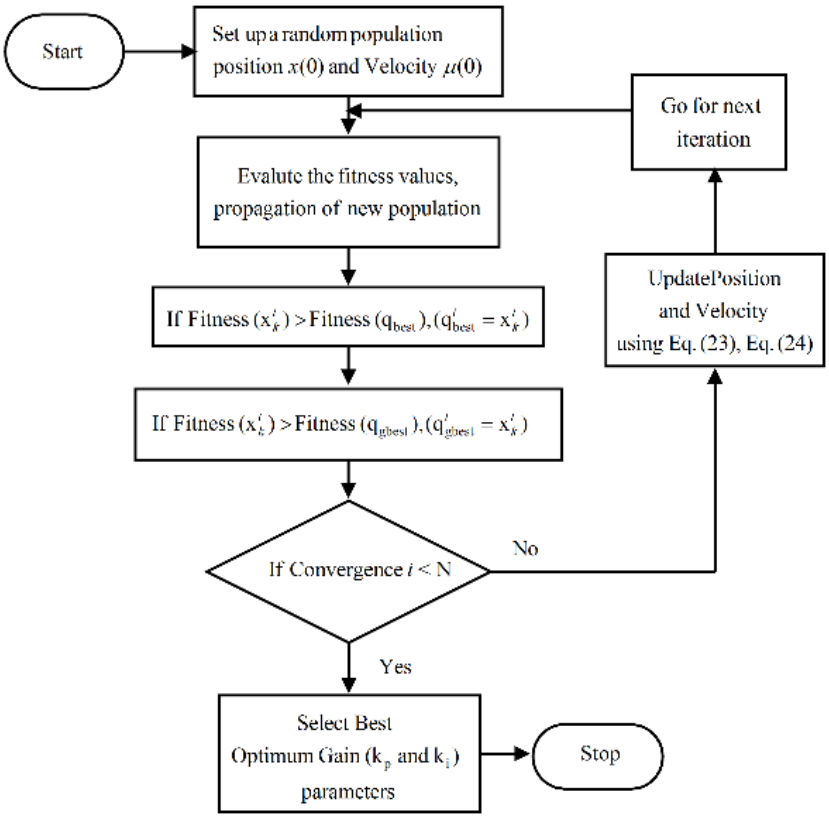

Fig. 3. Flow chart of PSO.

The flow chart of EPSO is shown in Fig. 4 and the process is as follows:

Step 1: Initialize the position and velocities of each particle
Step 2: Find the fitness of each particle
Step 3: Find the best position obtained by each particle
Update the particles with the best position obtained, re-initialise the position of each particle and analyse the lowest value obtained whether its new position is suitable, if it is yes, update its position otherwise assign other position randomly.

Step 4: Compare each particle global best fitness value with the q_{gbest}, if the present value is greater, update its fitness value.
Step 5: Check whether Eqs. (25) and (26) are satisfied, quit the iteration otherwise, return to step 3.

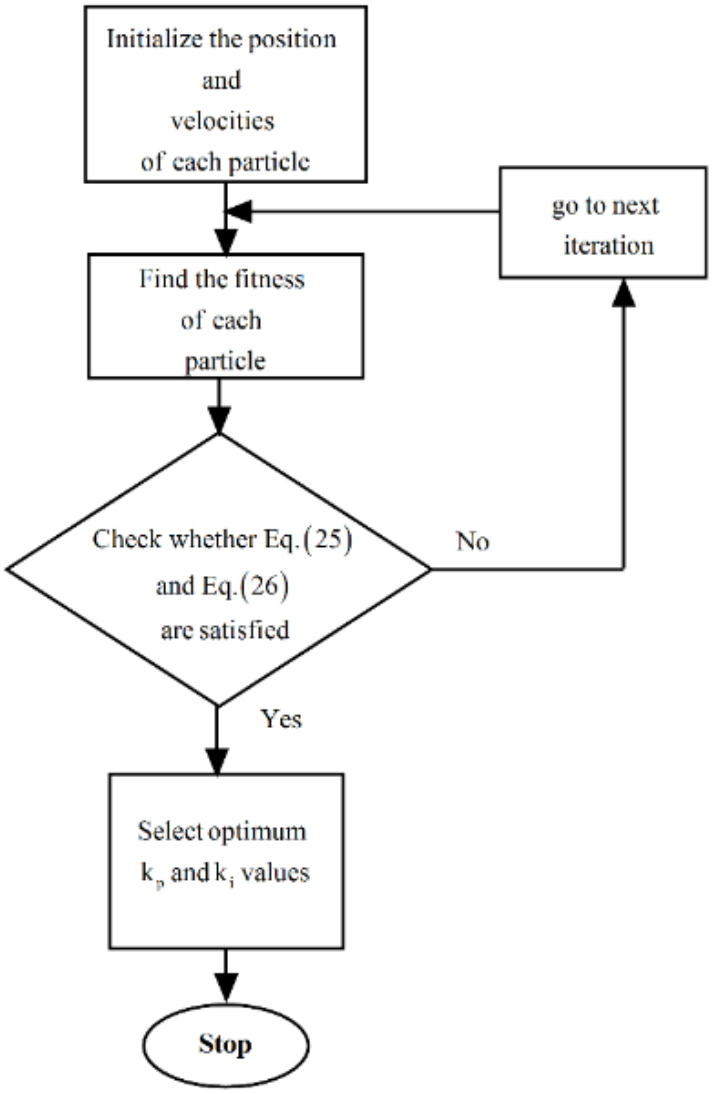

Fig. 4. Flow chart of EPSO.

3.2. Reference current generation

The literature enriched with different reference current generation techniques. However, the generalised *p-q* theory is robust, simple and easy to implement [3]. In generalised *p-q* theory, two type of approaches direct and indirect current control techniques. In this paper, the indirect current control method is adopted to mitigate current harmonics and reactive power.

Indirect current control technique

In indirect current control technique, Clarke's transformation is used for converting voltages and load currents from three-phase to two-phase. The orthogonal coordinates of supply voltages and load currents are as follows:

$$\begin{bmatrix} v_{s\alpha} \\ v_{s\beta} \end{bmatrix} = \sqrt{\frac{2}{3}} \begin{bmatrix} 1 & \frac{-1}{2} & \frac{-1}{2} \\ 0 & \frac{\sqrt{3}}{2} & \frac{-\sqrt{3}}{2} \end{bmatrix} \begin{bmatrix} v_{sa} \\ v_{sb} \\ v_{sc} \end{bmatrix} \tag{27}$$

$$\begin{bmatrix} i_{Load,\alpha} \\ i_{Load,\beta} \end{bmatrix} = \sqrt{\frac{2}{3}} \begin{bmatrix} 1 & \frac{-1}{2} & \frac{-1}{2} \\ 0 & \frac{\sqrt{3}}{2} & \frac{-\sqrt{3}}{2} \end{bmatrix} \begin{bmatrix} i_{Load,a} \\ i_{Load,b} \\ i_{Load,c} \end{bmatrix} \tag{28}$$

The orthogonal coordinates of supply voltages $v_{s\alpha}$ $v_{s\beta}$ and the load currents are $i_{Load,\alpha}$, $i_{Load,\beta}$, respectively. From Eqs. (27) and (28), the instantaneous power (*P*) can be calculated as:

$$P = v_{s\alpha} * i_{Load,\alpha} + v_{s\beta} * i_{Load,\beta} \tag{29}$$

The instantaneous real power has two components, dc ($\overline{p}$) and ac $\tilde{p}$ components. Since the source has to supply real power of the load, the DC component of power is used for generating the reference currents.

The two-phase reference currents are as follows:

$$i_{s\alpha}^{*} = \frac{v_{s\alpha}}{v_{s\alpha}^2 + v_{s\beta}^2} \overline{p} \quad \text{and} \quad i_{s\beta}^{*} = \frac{v_{s\beta}}{v_{s\alpha}^2 + v_{s\beta}^2} \overline{p} \tag{30}$$

These two-phase currents are converted into three-phase as follows:

$$\begin{bmatrix} i_{sa}^{*} \\ i_{sb}^{*} \\ i_{sc}^{*} \end{bmatrix} = \sqrt{\frac{2}{3}} \begin{bmatrix} 1 & 0 \\ \frac{-1}{2} & \frac{\sqrt{3}}{2} \\ \frac{1}{2} & \frac{-\sqrt{3}}{2} \end{bmatrix} \begin{bmatrix} i_{s\alpha}^{*} \\ i_{s\beta}^{*} \end{bmatrix} \tag{31}$$

The reference source currents are compared with the actual source currents, hence error will be generated. The generated error further processed through hysteresis current controller and produces switching pulses for SAPF.

4. Simulation Results and Discussion

The three-phase interleaved inverter based SAPF is modelled using MATLAB®/ Simulink environment. The simulation performance is tested under steady state and

transient conditions of load. The non-linear load is a full wave diode bridge rectifier with resistive and inductive elements (*R-L* load). Practically, the loads in the electrical power system are varying nature, therefore, the requirement of compensation varies. The amount of generating compensating current highly influenced by the DC-link voltage stabilisation. The non-linear load and interleaved inverter based SAPF parameters are tabulated in Appendix A.

The performance of proposed inverter topology is tested to work as SAPF in Section 4.1 under steady state condition of the non-linear load. Section 4.2 depicts the influence of the DC-link voltage on compensation performance of interleaved inverter based SAPF under dynamic-state of non-linear loads using PI, conventional PSO and EPSO algorithms.

4.1. Performance analysis under the steady-state condition of load

The performance parameters of the three-phase supply voltage (V_s), source current (I_s), phase-a load current ($I_{Load,a}$) and phase-a compensating current (I_{ca}) are shown in Fig. 5. It is observed that from Fig. 5, When the interleaved SAPF is switched on at $t = 0.1$ second. The proposed interleaved inverter is started working as a shunt active power. The harmonic spectrum of source current before compensation is 24.18% as shown in Fig. 6(a). The proposed EPSO based *p-q* control algorithm is tested in comparison with the conventional PI and PSO based control algorithms in terms of harmonic compensation and accuracy percentage of DC-link voltage. The DC-link voltage stabilisation has been reflected in the amount of harmonic compensation. The percentage THD level using EPSO, conventional PI and PSO based control algorithms are shown in Figs. 6(b), to (d), respectively.

It is contemplated from these results that the DC-link voltage set at its required reference value, which reduces switching power loss, power consumption on premises to operate the interleaved SAPF efficiently. The EPSO based *p-q* control algorithm adequately gives best-optimised solution for time-varying harmonics. Moreover, if any change in the harmonic currents and supply voltage, the DC-link voltage will be adjusted quickly as compared to the conventional PI and PSO based control algorithms. The convergence characteristics of the PI, PSO and EPSO based gain tunings are shown in Fig. 7.

The DC-link voltage has undergone to overshoot of 20 V when the interleaved SAPF is switched on at 0.1 second. The DC-link voltage has settled at 0.85 seconds. Where the PSO settled at 0.5 seconds and EPSO settled at 0.05 seconds. Hence, the proposed EPSO is reduced the overshoot and settling time. It is contemplated that the EPSO convergences faster due to the elimination of finding local maxima, where the PSO searches for local maxima. The percentage DC link voltage accuracy achieved by PI, conventional PSO and EPSO is 95.42%, 98.71% and 99.97%, respectively. It has been concluded that the proposed EPSO based control algorithm performed outstandingly by achieving the good harmonic compensation and percentage accuracy of DC-link voltage in comparison with the PI and PSO based algorithms. A complete performance comparison table of proposed EPSO, conventional PI and PSO based control algorithms are tabulated in Table 1.

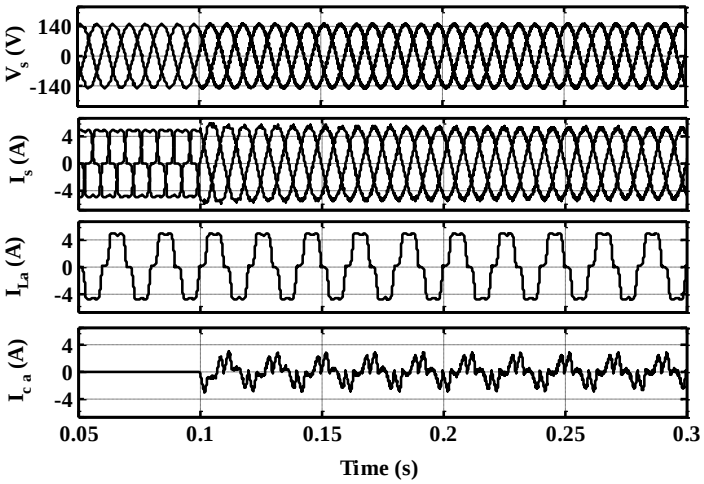

Fig. 5. Performance parameters of under steady state condition of the load.

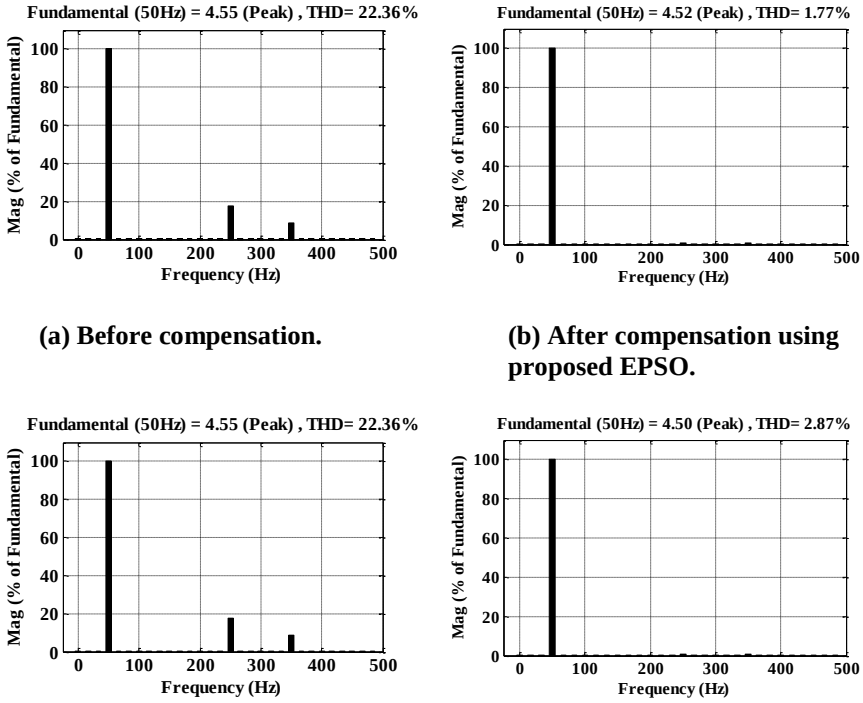

(a) Before compensation.

(b) After compensation using proposed EPSO.

(c) Using conventional PI.

(d) Using PSO.

Fig. 6. Harmonic spectrum of phase-a source current.

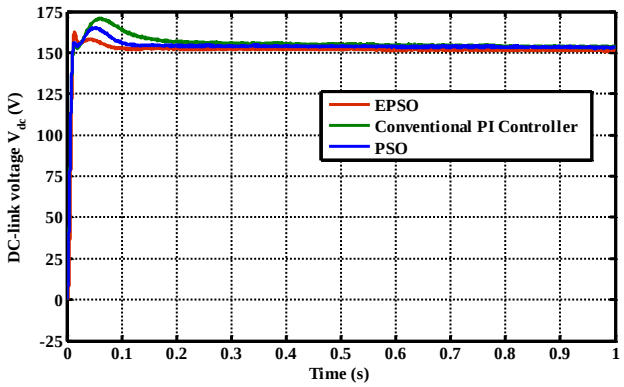

Fig. 7. DC-link voltage stabilization.

4.2. Performance analysis under transient condition of load

The proposed control algorithm is tested under a transient condition of the load to show the performance improvement. A fair comparison has been made in terms of overshoot, undershoot, response time, settling time and ripple voltage in-between proposed EPSO, PI controller and conventional PSO based algorithms. The performance of interleaved inverter based SAPF under sudden increase 50% of the load at t = 0.9 seconds and load removal at t = 1.4 seconds is shown in Fig. 8(a) and DC-link voltage stabilisation of EPSO, conventional PI and PSO are shown in Fig. 8(b). When the load increases, the capacitor voltage goes down to its reference value and vice versa. The conventional PI controller based algorithm performs overshoot of 10 V, undershoot of 10 V and response time of 2.15 seconds.

Similarly, the PSO based control algorithm performs overshoot of 5V, undershoot of 5 V and response time of 1.26 seconds. Where, the EPSO based control algorithm performs outstandingly with the lowest overshoot of 2 V, undershoot of 3 V and fastest response time of 0.02 seconds. Since the search process terminates the predefined maximum number of iterations completed or additional best solution is not obtained in conventional PSO. Moreover, the number of iterations and increase number of premature convergence of particle's best position will increase the complexity of the program and degrade the convergence speed. In contrary, the EPSO eliminates the premature convergence and reduce the computational complexity by avoiding each particle's best position obtained during the search process. It is proven that EPSO based *p-q* control algorithm performs outstandingly under the transient condition of the load with lower source current %THD, good accuracy, less overshoot, less undershoot and fast response time as tabulated in Table 1.

Table 1. Simulation comparison of algorithms on DC-voltage regulation.

Control algorithm for DC-voltage regulation	Steady state condition of load				Transient condition of load					
	%Accuracy of DC voltage	%THD			Settling time (s)	Overshoot (V)	Response time (s)	Undershoot (V)	Response time (s)	Ripple voltage (V)
		I_a	I_b	I_c						
PI controller	95.42	3.75	3.56	3.82	0.8	10	2.15	10	2.27	20
PSO	98.71	2.59	2.45	3.21	0.3	5	1.26	5	1.32	10
EPSO	99.97	1.27	1.25	1.29	0.05	2	0.7	3	0.21	4

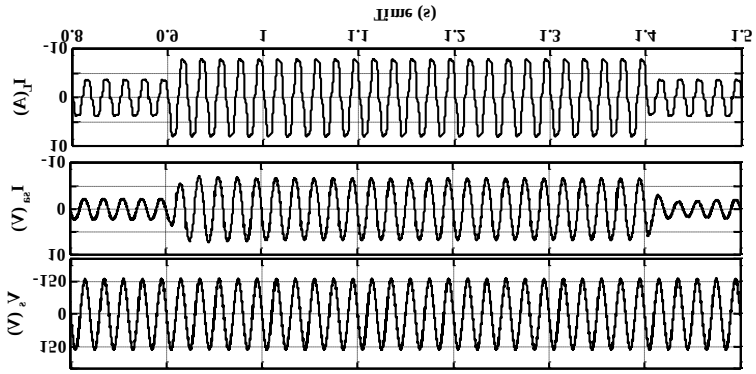

(a) Performance parameters under the transient condition of the load.

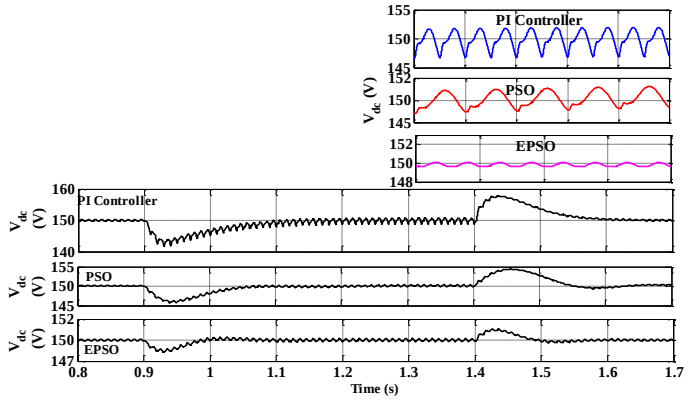

(b) Conventional PI, conventional PSO and EPSO based PI controller DC-link voltage stabilisation.

Fig. 8. Performance of interleaved SAPF under transient condition of load.

5. Experimental Results and Discussion

A laboratory prototype model is implemented using dSPACE 1104 controller to validate the performance of the proposed interleaved inverter based SAPF topology, EPSO based control algorithm in comparison with conventional PI, and PSO based algorithms. A three-phase diode bridge rectifier with RL load is connected as a non-linear load to create non-linearity in the system for testing of the proposed control algorithm. The laboratory prototype of the proposed SAPF is shown in Fig. 9. The dSPACE1104 controller has Real-Time Interface (RTI) block to connect the function model with Input/Output (I/O) interfaces through MATLAB®/ Simulink block. It configured with 250 MHz operating speed, 16-bit resolution of 8-parallel Digital to Analog Converters (DAC) and 4-multiplexed Analog to Digital Converters (ADC), 10 PWM outputs, 20 parallel digitals I/Os and 4-parallel 12-bit ADC channels. The required voltages and currents are sensed through high precision LEM voltage (LV 25-P) and current (LA 25-NP) sensors. The output of the sensors are in the range of very low values, therefore, a signal conditioning board is used for amplifying these signals to a certain range so that the ADCs can detect these signals.

The experimental testing is conducted on the reduced supply scale of 100 V_{rms}, which supplied from the three-phase auto-transformer. A digital signal oscilloscope (Tektronix TPS 2014B DSO; Beaverton, USA) and power quality analyser (Fluke 43B) is used for measurement of all waveforms and total harmonic distortions. Complete design parameters are shown in Appendix A.

1. Single-phase supply
2. Voltage and current sensors unit
3. Interleaved inverter
4. GATE driver circuit
5. Interfacing inductors
6. Bridge rectifier
7. dSPACE1104 controller
8. R-L load
9. Fluke 43B power quality analyse.
10. TPS 2014B DSO

Fig. 9. Laboratory prototype model of interleaved SAPF.

5.1. Performance analysis under steady-state condition

The performance of proposed interleaved inverter based SAPF is tested under the steady-state condition of the non-linear load with proposed EPSO based control algorithm in comparison with PI and conventional PSO based *p-q* control algorithms. The phase-a supply voltage and distorted source current before compensation are shown in Fig. 10(a). The three-phase distorted source currents are shown in Fig. 10(b) and their respective phase harmonic spectrums are shown in Figs. 11(a) to (c). The performance parameters of three-phase source currents ($i_{sa,}$ $i_{sb,}$, i_{sc}) after compensation using EPSO based *p-q* control algorithm is shown in Fig. 12(a) and their respective compensation currents are shown in Fig. 12(b). It is contemplated that the proposed interleaved inverter is working as a shunt active power filter. To compare the compensation effect of the three control techniques, harmonic spectral analysis have been carried out for source currents after compensation. The harmonic spectrum of source current after compensation of three control schemes are shown in Figs. 13(a) to (c), respectively. It observed in Fig. 13(a) that the proposed EPSO based control algorithm eliminates the premature convergence and reduces the computational complexity by avoiding each particle's best position obtained during the search process. It optimises the gain parameter values for variable harmonics presented in the system to tracks the DC-link reference voltage value. Therefore, the harmonic compensation level and percentage accuracy of DC-link voltage are improved. Whereas the PI controller fails to stabilize the DC-link voltage at its reference value due to variable harmonics presented in the system.

The harmonic compensation level is as shown in Fig. 13(b). It is observed in Fig. 13(c) that the PSO based tuning requires more of iterations to track the optimum values of gain values, which affect the dSPACE controller speed. Hence, gives atrocious results due failing to track its desire reference DC-link voltage value. A

complete performance comparison table of conventional PI, PSO and EPSO based control algorithms are shown in Table 2.

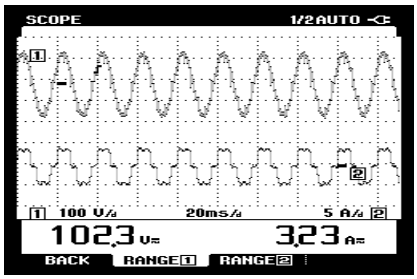

(a) Phase-a supply voltage and source current.

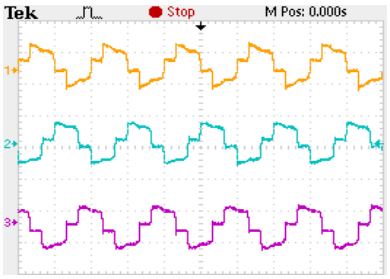

(b) Three-phase source currents i_{sa} (CH1), i_{sb} (CH2) and i_{sc} (CH3) (Y-axis: 3A/div; X-axis: 10ms) before compensation.

Fig. 10. Phase-a supply voltage and three-phase currents.

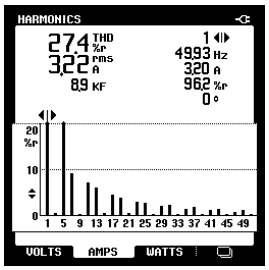

(a) phase-a source current.

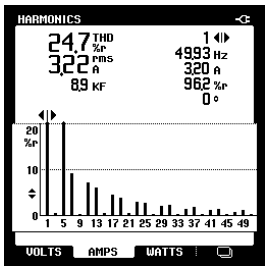

(b) phase-c source current.

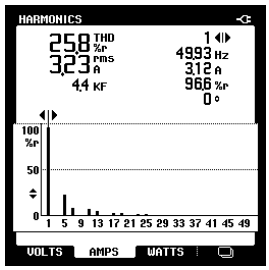

(c) phase-c source current.

Fig. 11. Harmonic spectrum of source currents before compensation.

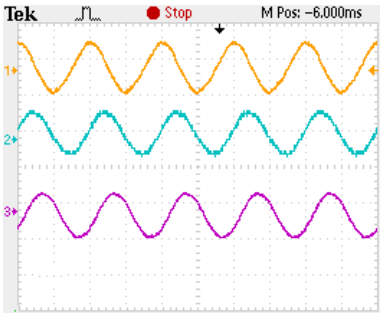

(a) i_{sa} (CH1), i_{sb} (CH2), i_{sc} (CH3)), (Y-axis: 3A/div; X-axis: 10ms).

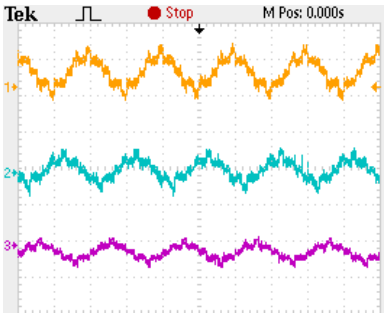

(b) compensating currents i_{ca} (CH1), i_{cb} (CH2), i_{cc} (CH3), (Y-axis: 300mA/div; X-axis: 10ms).

Fig. 12. Performance parameters interleaved SAPF after compensation.

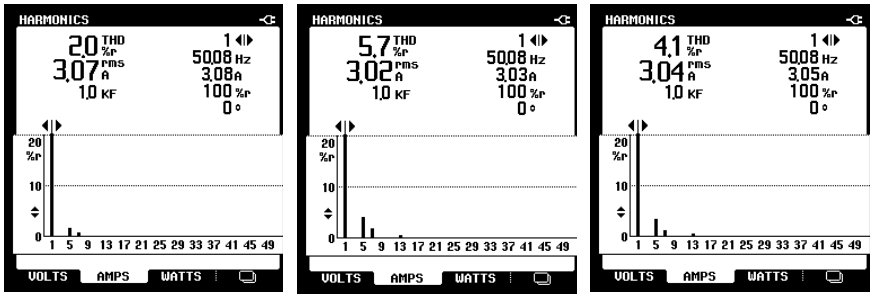

(a) EPSO. **(b) PI controller.** **(c) PSO.**

Fig. 13. Harmonic spectrual analysis of phase-a source current after compensation usage.

Table 2. Experimental comparison of algorithms on DC-voltage regulation.

Control algorithm for DC-voltage regulation	Steady-state condition of load		Transient condition of load					
	%Accuracy of DC voltage	%THD Source current after compensation	Settling time (s)	Overshoot (V)	Response time (s)	Undershoot (V)	Response time (s)	Ripples in DC-link voltage (V)
PI controller	95.42	5.7	2	10	1.15	12	2.27	15
PSO	98.71	4.1	0.7	5	0.5	8	1.32	10
EPSO	99.97	2.0	0.05	2	0.02	2	0.21	0.2

5.2. Performance analysis under transient condition

Extensive experimental analysis has been conducted on interleaved SPAF to test the robustness and effectiveness of the proposed EPSO based control algorithm during a transient condition of the load. The practical electrical power system experiences different hazardous load disturbances due to varying power demand, therefore, the DC-link capacitor undergoes inevitable disturbances. In such a scenario, the DC-link voltage has to be regulated at its normal reference value to ensure reliable and effective harmonic compensation. The effectiveness of the proposed EPSO based control algorithm is tested by sudden increment and decrement of the non-linear load.

The 56% of decrement and step load increment have been conducted in the laboratory. Hence, the load current increases from 2.15A to 3.8A and decreases from 3.8A to 2.15A are conducted in this paper. The response of conventional PI-based control algorithm is shown in Figs. 14(a) and 14(b), respectively. It is contemplated from these results that the when the load increases, the DC-link capacitor voltage undergoes down off its reference value to supply a sufficient amount of real power to the load. It recorded very poor results under this condition with undershoot of 10 V and very poor response time of 2.5 seconds. When the load decrement, the DC-link capacitor voltage increases with an overshoot of 12V and settle down to its reference value with a response time of 3.01 seconds. Therefore, the harmonic compensation affected in both dynamic conditions of the load with poor THD percentage.

The performance of PSO based control algorithm is tested under both step load increase and decrease are shown in Figs. 14(c) and (d) respectively. When the step load increases, the difference between the reference and real values of DC-link voltages are fed through the PSO algorithm to generate the optimised gain values to reduce the overshoot, undershoot and settling time. In this case, the PSO explores new domains in the searching space to entrap in local optimisation and causes to premature phenomena. Therefore, the PSO gives inevitable results under sudden step load increase, which undershoot of 10V and a settling time of 1.25 seconds. When step load decrease, the overshoot of 8V and settling time of 1.02 seconds. Thus, the harmonic compensation affected in both dynamic condition of the load with poor THD percentage of both step load increment and decrement.

The performance of the proposed EPSO based control algorithm under both step load increment and decrement are shown in Figs. 14(e) and (f) respectively. The proposed EPSO reduces the searching process to the local best position obtained by all the particles in the search process, which reduce the time of the search process and convergence time. The DC-link voltage undergo down to its reference value under step load increment, the proposed EPSO able to track the DC-link voltage to settle back to its reference value in 0.02 seconds with less undershoot voltage of 1 V. Similarly, DC-link voltage increases over reference value under step load decrease case.

The proposed EPSO gives best results to bring back to its reference value with less overshoot of 0.5 V and settling time 0.01 second. It is observed from all these results the proposed EPSO based control algorithm performs excellently under both steady state and dynamic-state load change conditions with high accuracy, very less response time, less overshoot and undershoot. By taking advantage of eliminating, the best solution obtained by all particles in the search process, which reduces the convergence speed and improve system efficiency. A complete performance comparison table is tabulated between conventional PI and conventional PSO and proposed EPSO control algorithms in Table 2.

(a) Step load increase, source current (CH2: Y-axis: 3A/div, X-axis: 25ms), load current (CH3- Y-axis: 3A/div, X-axis: 25ms), DC-link voltage (CH4: Y-axis-150V/div).

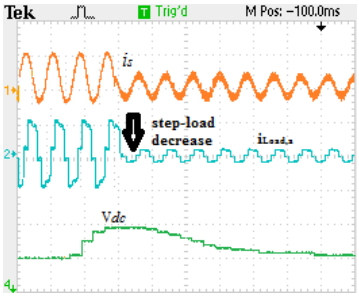

(b) Step load decrease, source current (CH1: Y-axis: 3A/div, X-axis: 25ms), load current (CH2- Y-axis: 3A/div, X-axis: 25ms), DC-link voltage (CH4: Y-axis-150V/div).

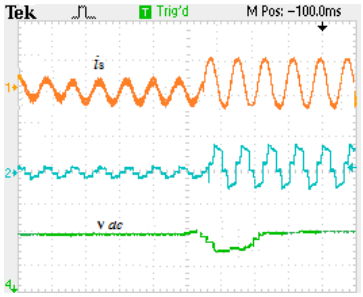

(c) Step load increase source current (CH1: Y-axis: 3A/div, X-axis: 25ms), load current (CH2- Y-axis: 3A/div, X-axis: 25ms), DC-link voltage (CH4: Y-axis-150V/div).

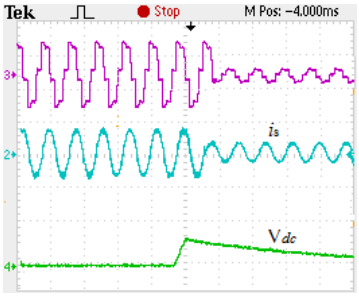

(d) Step load decrease, source current (CH2: Y-axis: 3A/div, X-axis: 25ms), load current (CH3- Y-axis: 3A/div, X-axis: 25ms), DC-link voltage (CH4: Y-axis-150V/div).

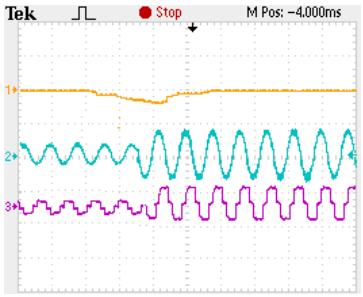

(e) Step load increase source current (CH2: Y-axis: 3A/div, X-axis: 25ms), load current (CH3- Y-axis: 3A/div, X-axis: 25ms), DC-link voltage (CH1: Y-axis-150V/div).

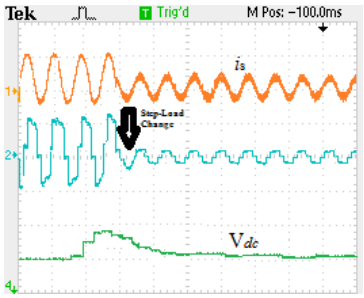

(f) Step load decrease, source current (CH1: Y-axis: 3A/div, X-axis: 25ms), load current (CH2- Y-axis: 3A/div, X-axis: 25ms), DC-link voltage (CH4: Y-axis-150V/div).

Fig. 14. Performance parameters of interleaved SAPF under transient condition of load using PI, PSO and EPSO based controllers.

6. Conclusion

Swarm intelligence techniques are applied to solve the multi-objective function of DC-link voltage stabilisation in interleaved SAPF. A fair comparison of the conventional PI, PSO and EPSO are tested under the steady state and transient condition of the load. The PI controller has been used for stabilising the DC-link voltage under steady state and transient conditions of the load. However, it gives poor results under sudden changing of loads. The PI controller gain parameters have been tuned to regulate the DC-link voltage using PSO and EPSO approaches. The performance improvement of proposed EPSO is compared with conventional PI tuning and PSO approaches using MATLAB®/ Simulink environment. A prototype model has been developed in the laboratory to validate the simulation results. It can be concluded from both simulation and hardware results that the proposed EPSO converges fast to find the best optimum PI gain parameters under steady state and transient condition of the load with less overshoot and undershoot.

Nomenclature

C_{dc}	DC-link capacitor, micro Farad
I_{Load1}, $I_{Load,h}$,	Peak values of fundamental and harmonic components of load currents
i_f	Compensating current, Ampere
i_{Load}	Load current, Ampere
$i_{Load,h}$	Harmonic component of load current, Ampere
i_{Load1}	Fundamental load current, Ampere
$i_{Load,\alpha}$ $i_{Load,\beta}$,	α-β coordinates of load currents, Ampere
i_{sa}^*, i_{sb}^*, i_{sc}^*	Generated reference source currents, Ampere
$i_{s\alpha}^*$, $i_{s\beta}^*$	α-β coordinates of source currents, Ampere
K_i	Integral gain constant
K_p	Proportional gain constant
L_a	Phase-a interfacing inductor, milli Henry
m	Modulation Index
$\overline{p}$, $\tilde{p}$	DC and AC component of powers, Watt
u_k^i	Velocity of ith particle
V_{cmax}	Maximum inverter voltage, Volts
V_{cmin}	Minimum inverter voltage, Volts
V_{dc}	DC-link capacitor voltage, Volts
$V_{dc,avg}^*$	Average DC-link voltage, Volts
V_{sn}	Peak-value of supply voltage, Volts
v_c	Inverter voltage, Volts
v_{c1}	Fundamental component of inverter voltage, V
v_{cn}	Effective fundamental nth component of inverter voltage, Volts
v_L	Voltage drop across interfacing inductor, Volts
v_s	Supply voltage, Volts
$v_{s\alpha}$, $v_{s\beta}$	α-β coordinates of supply voltages, Volts
W_{dc}	Energy stored in DC-link capacitor
W_{dc}^*	Reference Energy stored in DC-link capacitor
x_k^i	Position of i^{th} particle

Greek Symbols

ΔW_{dc}	Energy loss
η	Random number
λ_1	Constant
λ_2	Constant
ϕ	Initial phase component of supply voltage
φ	Initial phase component of inverter voltage
χ	Coefficient of inertia
ω	Fundamental angular frequency

Abbreviations	
APF	Active Filter
EPSO	Enhanced Particle Swarm Optimization
PSO	Particle Swarm Optimization
SAPF	Shunt Active Power Filter

References

1. Bollen, M.H.J. (1999). *Understanding power quality problems: Voltage sags and interruptions*. New Jersey: IEEE Press.
2. Arrillaga, J.; and Watson, N.R. (2004). *Power system harmonics*. Chichester, West Sussex: John Wiley & Sons, Ltd.
3. Gursoy, M.I.; Yilmaz, A.S.; and Ustun, S.V. (2018). A practical real-time power quality event monitoring applications using discrete wavelet transform and artificial neural network. *Journal of Engineering Science and Technology* (*JESTEC*), 13(6), 1764-1781.
4. Kazem, H.A. (2013). Harmonic mitigation techniques applied to power distribution networks. *Advances in Power Electronics*. Article ID 591680. 10 pages.
5. Gali, V.K.; Gupta, N.; and Gupta, R.A. (2017). Mitigation of power quality problems using shunt active power filters: A comprehensive review. *Proceedings of 12th IEEE Industrial Electronics and Applications (ICIEA*). Siem Reap, Cambodia, 1100-1105.
6. Sun, P.; Liu, C.; Lai, J.-S.; Chen, C.-L.; and Kees, N. (2012).Three-phase dual-buck inverter with unified pulse width modulation. *IEEE Transactions on Power Electronics*, 27(3), 1159-1167.
7. Chen, L.; and Peng. F.Z. (2008). Dead-time elimination for voltage source inverters. *IEEE Transactions Power Electronics*, 23(2), 574-580.
8. Goluszek, D. (2001). Two stage power converter with interleaved buck regulators. Communications & Power Industries Inc. *United States Patent. No. US 6,211,657 BI*. 11 pages.
9. Patel, R.; and Panda, A.K. (2014). Real time implementation of PI and fuzzy logic controller based 3-phase 4-wire interleaved buck active power filter for mitigation of harmonics with i_d–i_q control strategy. *International Journal of Electrical Power & Energy Systems*, 59, 66-78.
10. Panda, A.K.; and Patel, R. (2015). Adaptive hysteresis and fuzzy logic controlled-based shunt active power filter resistant to shoot-through phenomenon. *IET Power Electron*, 8(10), 1963-1977.
11. Motahhir, S.; El Ghzizal, A.; Sebti, S.; and Derouich, A. (2017). MIL and SIL and PIL tests for MPPT algorithm. *Cogent Engineering*, 4(1), 1-18.
12. Vardar, K.; Akpınar, E.; and Surgevil, T. (2009). Evaluation of reference current extraction methods for DSP implementation in active power filters. *Electric Power System Research*, 79(10), 1342-1352.
13. Gali, V.; Gupta, N.; and Gupta, R.A. (2017). Improved dynamic performance of shunt active power filter using particle swarm optimization. *Proceedings of the IEEE International Conference on Intelligent Techniques in Control, Optimization and Signal Processing (INCOS)*. Srivilliputhur, India, 1-7.

14. Vijayakumar, G.; and Anita, R. (2015). Photovoltaic based shunt active filter for power quality improvement using icosφ theory. *Journal of Engineering Science and Technology* (*JESTEC*), 10(11), 1422-1440.
15. Singh, B.; Chandra, A.; and Al-Haddad, K. (2015). *Power quality: Problems and mitigation techniques*. Chichester, West Sussex: John Wiley & Sons, Ltd.
16. Singh, B.; and Kumar, S. (2010). Modified power balance theory for control of DSTATCOM. *Proceedings of the Joint International Conference on Power Electronics, Drives and Energy Systems (PEDES) and 2010 Power India*. New Delhi, India, 1-8.
17. Rao, U.K.; Mishra, M.K.; and and Ghosh, A. (2008). Control strategies for load compensation using instantaneous symmetrical component theory under different supply voltages. *IEEE Transactions on Power Delivery*, 23(4), 2310-2317.
18. Singh, B.; and Arya, S.R. (2013). Implementation of single-phase enhanced phase-locked loop-based control algorithm for three-phase DSTATCOM. *IEEE Transactions on Power Delivery*, 28(3) 1516-1524.
19. Li, X.; He, H.; Lu, J.; and Liang, Z. (2015). Modified synchronous reference frame method for active power filter under asymmetric and distorted supply voltages condition. *Proceedings of IEEE International Conference on Industrial Informatics-Computing Technology, Intelligent Technology, Industrial Information Integration*. Wuhan, China, 1-5.
20. Mahanty, R. (2014). Indirect current controlled shunt active power filter for power quality improvement. *International Journal of Electrical Power & Energy System*, 62, 441-449.
21. Akagi, H.; Watanabe, E.H.; and Aredes, M. (2007). *Instantaneous power theory and* applications *to power conditioning.* Piscataway, New Jersey: IEEE Press.
22. Wang, Y.; Xie, Y.-X.; and Liu, X. (2015). Analysis and design of DC-link voltage controller in shunt active power filter. *Journal of Power Electronics*, 15(3), 763-774.
23. Zainuri, M.A.A.M.; Radzi, M.A.M.; Soh, A.C.; Mariun, N.; Rahim, N.A. (2016). DC-link capacitor voltage control for single-phase shunt active power filter with step size error cancellation in self-charging algorithm. *IET Power Electronics*, 9(2), 323-335.
24. Chaoui, A., Gaubert, J.P.; Krim, F.; and Champenois, G. (2007). PI controlled three-phase shunt active power filter for power quality improvement. *Electric Power Components and Systems*, 35(12), 1331-1344.
25. Mahni, T.; Benchouia, M.T.; Ghamri, A.; and Golea, A. (2018). Three-phase four-wire shunt active filter under unbalanced loads with back stepping and PI controllers. *Australian Journal of Electrical and Electronics Engineering*, 14(1-2), 41-47.
26. Kumar, P.; and Mahajan, A. (2009). Soft computing techniques for the control of an active power filter. *IEEE Transactions on Power Delivery*, 24(1), 452-461.
27. Panda, A.K.; and Mikkili, S. (2012). Fuzzy logic controller based shunt active filter control strategies for power quality improvement using different fuzzy M.F.s. *International Journal of Emerging Electric Power Systems*, 13(5). Article 2.
28. Benchouia, M.T.; Ghadbane, I.; Golea, A.; Srairi, K.; and Benbouzid, M.E.H. (2015). Implementation of adaptive fuzzy logic and PI controllers to regulate

the DC bus voltage of shunt active power filter. *Applied Soft Computing*, 28, 125-131.

29. El-Saady, G.; El-Sayed, A.-H.; Ibrahim, E.A.; and Abdul-Ghaffar, H.I. (2015). Harmonic compensation using on-line bacterial foraging optimization based three-phase active power filter. *WSEAS Transactions on Power Syst*ems, 10, 73-81.
30. Babu, T.S.; Priya, K.; Maheswaran, D.; Kumar, K.S.; and Rajasekar, N. (2015). Selective voltage harmonic elimination in PWM inverter using bacterial foraging algorithm. *Swarm and Evolutionary Computation*, 20, 74-81.
31. Mishra, S.; and Bhende, C.N. (2007). Bacterial foraging technique-based optimized active power filter for load compensation. *IEEE Transactions on Power Delivery*, 22(1), 457-465.
32. Gali, V.; Gupta, N.; and Gupta, R.A. (2017). Improved dynamic performance of shunt active power filter using particle swarm optimization. *Proceedings of the IEEE International Conference on Intelligent Techniques in Control, Optimization and Signal Processing (INCOS*). Srivilliputhur, India, 1-7.
33. Fereidouni, A.; Masoum, M.A.S.; Mehr, T.H.; and Moghbel, M. (2014). Improving performance of shunt active power filter with hysteresis-based direct current control using particle swarm optimization. *Australian Journal of Electrical and Electronics Engineering*, 11(4), 357-365.
34. Patnaik, S.S.; and Panda, A.K. (2013). Real-time performance analysis and comparison of various control schemes for particle swarm optimization-based shunt active power filters. *International Journal Electrical Power & Energy System*, 52, 185-197.
35. Tian, D.; and Shi, Z. (2018). MPSO: Modified particle swarm optimization and its applications. *Swarm and Evolutionary Computation*, 41, 49-68.

Appendix A

The simulation and experimental study parameters.

Parameters	Symbol	Simulation	Experimental
Supply voltage	v_s	100 V RMS (50 Hz)	100 V RMS (50 Hz)
Series resistance	R_S	0.1 Ω	0.1 Ω
Series inductance	L_S	0.5 mH	0.5mH
Interfacing resistance	$Ra1$, $Ra2$, $Rb1$, $Rb2$	0.7 Ω	0.7 Ω
Interfacing inductor	L_{a1}, L_{a2}, L_{b1}, L_{b2}	2 mH	2mH
DC-link capacitor	C_{dc}	1000 µF	1000 µF
DC-link capacitor voltage	V_{dc}	150 V	150 V
PI controller values	k_p, k_i	0.1, 1	0.1, 1
Non-linear Resistive Load	R_L	16 Ω (initially)	16 Ω (initially)
Non-linear inductive Load	L_L	30 mH	30 mH